JVI Journals.ASM.org

Immunodeficient Mouse Models with Different Disease Profiles by *In Vivo* Infection with the Same Clinical Isolate of Enterovirus 71

Chun-Che Liao,[a,b] An-Ting Liou,[b,c,h] Ya-Shu Chang,[b] Szu-Yao Wu,[b,d] Chih-Shin Chang,[b,d] Chien-Kuo Lee,[e] John T. Kung,[f] Pang-Hsien Tu,[b] Ya-Yen Yu,[g] Chi-Yung Lin,[g] Jen-Shiou Lin,[g] Chiaho Shih[a,b,c]

Graduate Institute of Life Sciences, National Defense Medical Center, Taipei, Taiwan[a]; Institute of Biomedical Sciences, Academia Sinica, Taipei, Taiwan[b]; Taiwan International Graduate Program (TIGP) in Molecular Medicine, National Yang-Ming University and Academia Sinica, Taipei, Taiwan[c]; Institute of Microbiology and Immunology, National Yang-Ming University, Taipei, Taiwan[d]; Institute of Immunology, National Taiwan University, Taipei, Taiwan[e]; Institute of Molecular Biology, Academia Sinica, Taipei, Taiwan[f]; Section of Clinical Virology and Molecular Diagnosis, Department of Laboratory Medicine, Changhua Christian Hospital, Changhua, Taiwan[g]; Institute of Biochemistry and Molecular Biology, National Yang-Ming University, Taipei, Taiwan[h]

ABSTRACT

Like poliovirus infection, severe infection with enterovirus 71 (EV71) can cause neuropathology. Unlike poliovirus, EV71 is often associated with hand-foot-and-mouth disease (HFMD). Here we established three mouse models for experimental infection with the same clinical isolate of EV71. The NOD/SCID mouse model is unique for the development of skin rash, an HFMD-like symptom. While the NOD/SCID mice developed limb paralysis and death at near-100% efficiency, the gamma interferon receptor knockout (*ifngr* KO) and *stat-1* knockout mice exhibited paralysis and death rates near 78% and 30%, respectively. Productive infection with EV71 depends on the viral dose, host age, and inoculation route. Levels of infectious EV71, and levels of VP1-specific RNA and protein in muscle, brain, and spinal cord, were compared side by side between the NOD/SCID and *stat-1* knockout models before, during, and after disease onset. Spleen fibrosis and muscle degeneration are common in the NOD/SCID and *stat-1* knockout models. The main differences between these two models include their disease manifestations and cytokine/chemokine profiles. The pathology of the NOD/SCID model includes (i) inflammation and expression of viral VP1 antigen in muscle, (ii) increased neutrophil levels and decreased eosinophil and lymphocyte levels, and (iii) hair loss and skin rash. The characteristic pathology of the *stat-1* knockout model includes (i) a strong tropism of EV71 for the central nervous system, (ii) detection of VP1 protein in the Purkinje layer of cerebellar cortex, pons, brain stem, and spinal cord, (iii) amplification of microglial cells, and (iv) dystrophy of intestinal villi. Our comparative studies on these new models with oral or intraperitoneal (i.p.) infection underscored the contribution of host immunity, including the gamma interferon receptor, to EV71 pathogenesis.

IMPORTANCE

In the past decade, enterovirus 71 (EV71) has emerged as a major threat to public health in the Asia-Pacific region. Disease manifestations include subclinical infection, common-cold-like syndromes, hand-foot-and-mouth disease (HFMD), uncomplicated brain stem encephalitis, severe dysregulation of the autonomic nerve system, fatal pulmonary edema, and cardiopulmonary collapse. To date, no effective vaccine or treatment is available. A user-friendly and widely accessible animal model for researching EV71 infection and pathogenesis is urgently needed by the global community, both in academia and in industry.

In the past decade, enterovirus 71 (EV71) has emerged as a major threat to public health in the Asia-Pacific region (1, 2). As a member of the *Picornaviridae*, EV71 is related to poliovirus (3), hepatitis A virus (EV72) (4), and coxsackieviruses (5). It is likely that both viral and host factors could contribute to the diverse pathogenesis profiles, ranging from subclinical infection, common-cold-like syndromes, and hand-foot-and-mouth disease (HFMD) to uncomplicated brain stem encephalitis, severe dysregulation of the autonomic nerve system, fatal pulmonary edema, and cardiopulmonary collapse. To date, no effective vaccine or treatment is available (6, 7). A user-friendly and widely accessible animal model for EV71 infection would be most convenient for the research community.

By serial passages through mouse brain, Wang et al. (8) reported experimental infection of newborn ICR mice with a mouse-adapted EV71 strain, MP4. In general, newborn mice (1 to 2 days old) are difficult to handle technically. A further adapted strain, M2, can infect 12- to 14-day-old ICR mice (9). However, it remains unclear if adaptive mutations associated with the various mouse-adapted strains can be found in natural human infection. For example, a G145E adaptive mutation at the VP1 of a mouse-adapted EV71 strain is essential for hind-limb paralysis in 3- to 4-week-old NOD/SCID mice (10). Cynomolgus monkeys could also serve as an animal model for the study of EV71 pathogenesis (11). However, monkeys are not a convenient model and are not easily accessible for most laboratories. AG129 mice are known to

Received 12 March 2014 **Accepted** 10 August 2014
Published ahead of print 20 August 2014
Editor: K. Kirkegaard
Address correspondence to Chiaho Shih, cshih@ibms.sinica.edu.tw.
C.-C.L. and A.-T.L. contributed equally to this article.
Supplemental material for this article may be found at http://dx.doi.org/10.1128/JVI.00692-14.

doi:10.1128/JVI.00692-14

lack type I and II interferon receptors (IFNR) and therefore are severely defective in innate immunity. Khong et al. (12) reported that AG129 mice were susceptible to non-mouse-adapted EV71 infection via the intraperitoneal (i.p.) and oral routes. Infected mice developed limb paralysis and death. An adapted strain of EV71 that can infect adult AG129 mice has been reported (13). Yamayoshi et al. (14) reported that human scavenger receptor B2 (SCARB2) can function as a receptor for EV71 entry *in vitro*. Similarly, Nishimura et al. (15) reported that human P-selectin glycoprotein ligand-1(PSGL-1) can also facilitate EV71 infection *in vitro*. Recently, it was reported that human SCARB2 (hSCARB2) transgenic (Tg) mice can serve as an animal model of EV71 infection (16, 17). While these receptor Tg mice can suffer limb paralysis upon i.p. injection with EV71, no typical symptoms of HFMD with skin rash were observed. In fact, acute flaccid paralysis is a rare clinical event (0.31%) in natural human EV71 infection (1, 18). Furthermore, limb paralysis is not a unique phenotype of EV71; many other viruses can also cause limb paralysis in animal models (19, 20). Another important issue in the current SCARB2 receptor Tg model is its lack of oral infection (17). While oral infection was observed in another SCARB2 Tg model, the efficiency appeared to be very low using a so-called Isehara strain of EV71 (success rate, only 2/50 in three experiments) (16). Therefore, there is an urgent need to develop an animal model that can closely mimic human natural infection, for example, producing the HFMD-like phenotype via a more-efficient oral infection.

In the literature, the same animal model was infected with different genotypes of EV71 (16, 17). In contrast, the use of the same viral strain for the infection of different animal models remains to be explored. Considering the outbred human population, the effect of host genetic factors on viral pathogenesis needs to be investigated.

In this study, by using the same clinical isolate of EV71 in three newly established animal models susceptible to EV71 infection, we demonstrated that these models with different genetic backgrounds exhibited different disease profiles. Interestingly, in nonobese diabetic mice with severe combined immunodeficiency disease (NOD/SCID mice), the infection and disease manifestations appeared to be more systemic in multiple tissues than neurotropic. In particular, spleen fibrosis, muscle inflammation and destruction, and abnormal hematological features were evident in the NOD/SCID model. Notably, no productive infection and disease were observed when UV-treated EV71 was inoculated. A robust oral infection system was established using the NOD/SCID mouse model. In contrast, in the *stat-1* knockout (KO) model, EV71 infection was highly neurotropic, with striking VP1 expression and massive microglial cell amplification in the central nervous system (CNS). Both pons and cerebellar Purkinje cells were strongly targeted by EV71, suggesting a retrograde axonal transport mechanism. While the strong neurotropism of EV71 in the *stat-1* KO model resembles what has been described in patients, our studies in the NOD/SCID model suggest that EV71 might also cause systemic-infection-like symptoms. Most likely, both muscle and CNS infections could contribute to limb paralysis. We report here that skin rash in NOD/SCID mice can be observed after inoculation by the i.p. or oral route. Furthermore, by using a gamma interferon (IFN-γ) receptor knockout (*ifngr* KO) mouse model, we demonstrated that the IFN-γ receptor is likely to be critical for protection from EV71 infection and pathogenesis. Our new models provide a novel tool both for basic science research and for the development of antivirals and vaccine candidates.

MATERIALS AND METHODS

Ethics statement. All animal experiments were conducted under protocols approved by the Academia Sinica Institutional Animal Care and Utilization Committee (ASIACUC protocol number 2010003). Research was conducted in compliance with the principles stated in the *Guide for the Care and Use of Laboratory Animals* (21).

Cells and virus preparation. Human rhabdomyosarcoma (RD) cells (ATCC CCL-136) were grown in Dulbecco's modified Eagle medium (DMEM; Gibco) with 10% fetal bovine serum (FBS; HyClone) and 1% penicillin-streptomycin (Gibco). EV71 clinical isolates were kindly provided by the Section of Clinical Virology and Molecular Diagnosis, Department of Laboratory Medicine, Changhua Christian Hospital. For virus preparation, RD cells were infected with EV71 clinical isolate F23 at a multiplicity of infection (MOI) of 0.01 and were maintained in DMEM with 0.2% FBS. The virus was harvested by three free-thaw cycles and was clarified by centrifugation at 3,000 × *g* for 30 min at 4°C. Virus in clarified medium was concentrated by ultracentrifugation in Beckman SW28 rotors at 121,896 × *g* (26,000 rpm) for 4 h at 4°C with a 30% sucrose cushion and was resuspended in phosphate-buffered saline (PBS). The virus titer was determined by a plaque assay before animal infection. In brief, RD cell monolayers in 6-well plates (SPL Life Sciences) were infected with 10-fold serially diluted virus in DMEM. After incubation at 37°C under 5% CO_2 for 1 h, the virus was removed, and the cells were covered with 4 ml of 0.3% agarose (Lonza) in DMEM with 0.2% FBS. After incubation at 37°C under 5% CO_2 for 3 days, the cells were fixed by 3.7% formalin (Merck) for 1 h and were stained with 0.5% crystal violet. For the UV inactivation experiment, purified EV71 was UV irradiated at 750 mJ/cm^2 using a CL-1000 UV cross-linker (UVP). The residual viral titer after UV treatment was determined by a plaque assay.

Experimental infection and antibody treatment. NOD/SCID mice were purchased from Lasco Co., Ltd. (Taiwan). The *stat-1* KO mice and *ifngr* KO (129/Sv/Ev inbred) mice were provided by Chien-Kuo Lee and John Kung, respectively. Mice were housed under specific-pathogen-free conditions in individual ventilated cages. One-week-old NOD/SCID or *stat-1* KO mice were infected via the intraperitoneal (i.p.) or subcutaneous (s.c.) route with EV71 clinical strain F23 at a dose of 10^5 to 10^8 PFU/mouse. For oral infection, 10^8 PFU of EV71 was injected into each NOD/SCID mouse (3 days old) with a 24-gauge feeding tube after 6 h of fasting. Neutralizing antibodies against the IFN-α receptor or IFN-γ (Bio X Cell) were i.p. injected at a dose of 150 μg/mouse into 1-week-old wild-type C57BL/6 mice (NAR Labs, Taiwan). EV71 infection (10^8 PFU/mouse) was carried out via the i.p. route. The neutralizing antibody against the IFN-α receptor was injected 1 day before EV71 inoculation, followed by repetitive antibody treatments on days 1 and 3 postinoculation (1 and 3 dpi). The neutralizing antibody against IFN-γ was coinjected with EV71, followed by repetitive antibody treatments on 1 and 2 dpi. Mice were monitored daily for disease manifestations.

Histopathological and immunohistochemical (IHC) staining. Euthanatized mice were perfused transcardially with PBS followed by 10% neutral buffered formalin (Chin I Pao Co., Ltd., Taiwan). Tissues were fixed in 10% neutral buffered formalin overnight. Fixed tissues were paraffin embedded, sliced, and stained with hematoxylin and eosin (H&E) or Masson's trichrome stain by the Pathology Core Laboratory, IBMS, Academia Sinica. Xylene and ethanol were used for deparaffinization and rehydration. Retrieval buffer (pH 6.0) and endogenous enzyme blocker (both from Dako) were used for antigen retrieval and blocking steps. The slides were washed with PBS containing 0.1% Tween 20 (PBST) and were incubated with an anti-VP1 (Abnova), anti-F4/80 (GeneTex, Taiwan), anti-keratin 6, anti-keratin 14 (Covance), anti-pan-collagen type I (Millipore), or anti-IBA1 (GeneTex, Taiwan) antibody. These slides were washed with PBST and were incubated with an anti-rabbit or anti-rat secondary antibody (both from Dako). A diaminobenzidine (DAB) sys-

tem (Dako) was used to present the signal of each antigen. Sections were counterstained with hematoxylin (J.T. Baker) and were mounted with mounting reagent (Muto Pure Chemicals).

Tissue sampling and virus titration. After euthanasia, blood samples were collected by heart puncture prior to PBS perfusion. Organs and tissues were harvested, weighed, and homogenized by a mechanical homogenizer (Next Advance) in PBS. Viruses in supernatants of clarified homogenates and blood serum were routinely first amplified by passaging the tissue-derived virus through the RD cells for one round (24 h) before reinfection with RD cells for the plaque assay. Viral titers were determined by plaque assays and are expressed as PFU per gram (for tissue) or per milliliter (for sera).

Real-time reverse transcription-PCR (RT-PCR). Total RNAs of tissue homogenates were extracted with a WelPrep cell/tissue RNA kit (WelGENE), and were used for reverse transcription by a High-Capacity cDNA reverse transcription kit (Applied Biosystems). The synthetic cDNA was subjected to real-time quantitative PCR (qPCR) analysis by an ABI 7500 system with a Power SYBR green PCR master kit (both from Applied Biosystems). The specific primers for VP1 were CTAGAGGGTACCACC AATCC (forward) and AACCTGGCCAGTAGGAGT (reverse). The primer sequences of the internal control, glyceraldehyde-3-phosphate dehydrogenase (GAPDH), were GTTCCTACCCCCAATGTG (forward) and CAACCTGGTCCTCAGTGTAG (reverse).

Cytokine quantification. Cytokines in tissue homogenates were measured by a Procarta immunoassay kit (Affymetrix) according to the manufacturer's instructions. The sensitivity of detection of the various cytokines is described in the manufacturer's protocol.

CBC. Blood samples from infected mice were collected with 1.5 mg/ml of Na_2EDTA. The complete blood counts (CBC) of mice were conducted with an Abbott Cell-Dyn 3700 system.

Immunoblotting. Radioimmunoprecipitation assay (RIPA) buffer was used to extract protein from tissue homogenates. VP1 protein and tubulin were detected by an anti-VP1 antibody (Abnova) and an anti-tubulin antibody (GeneTex, Taiwan), respectively.

Statistical analysis. All experimental results from two to six independent experiments were analyzed by Student's *t* test. Two-way analysis of variance (ANOVA) was used to analyze the differences in HFMD-like syndromes and limb paralysis between oral and nonoral routes of infection.

RESULTS

Host immunity plays an important role in resistance and clearance of viral infection. For example, AG129 mice deficient in interferon (IFN-α/β and IFN-γ) signaling can be infected with EV71 *in vivo* (12). To address the issue of immunity and host defense against EV71, we tested several immunodeficient mouse strains for susceptibility to infection with clinical isolates of EV71 (Fig. 1A). To our surprise, neither IFN-α receptor knockout (*ifnar* KO) mice nor complement C5-deficient FVB mice could support EV71 infection. Instead, we observed successful infection of *stat-1* KO, NOD/SCID, and IFN-γ receptor knockout (*ifngr* KO) mice. Because we succeeded with the *ifngr* KO model only very recently, our more detailed characterizations focused primarily on the other two models. *stat-1* KO mice lack the STAT1 gene and are defective in IFN signaling (22), while NOD/SCID mice are known to be defective in the innate immunity of NK cells as well as the humoral immunity of T and B cells (23).

We injected EV71 (genotype B5, strain F23 [see Materials and Methods]) i.p. into 1-week-old NOD/SCID mice and monitored the time course of viral titers in the sera postinoculation (Fig. 1B). On day 3 postinoculation (3 dpi), viral titers reached a peak, suggesting that EV71 was replicating in the inoculated mice. However, viral titers began to decline on day 4 and became undetectable on day 8. We noted occasional (36%) hair loss (Fig. 1C) on days 2 to 6 and skin rash (Fig. 1D; see also Fig. S1A in the supplemental material) after 9 dpi. In contrast, near-100% limb paralysis was observed on days 8 to 12 postinoculation (Fig. 1E; see also Fig. S1B in the supplemental material). These phenomena were not detected in PBS-injected NOD/SCID controls. To test whether the disease manifestation could be caused by the input virus without viral proliferation *in vivo*, we performed a UV inactivation experiment (Materials and Methods). Inoculation of UV-inactivated virus produced neither plaques in RD cells (data not shown) nor death and clinical scores in NOD/SCID mice (Fig. 1F and G). This result strongly supports the correlation between viral replication (Fig. 1B) and pathogenesis (Fig. 1F and G).

The survival rate and clinical score were dependent on the viral dose ($\leq 10^6$ PFU/mouse versus 10^7 to 10^8 PFU/mouse) (Fig. 1H and I), host age (1 week versus 2 to 4 weeks) (Fig. 1J and K), and injection route (oral, s.c., or i.p.) (Fig. 1L and M).When mice were inoculated with a lower dose of EV71 (below 10^6 PFU), or at an older age (2 to 4 weeks), no death or clinical score was ever observed (Fig. 1H to K). Oral infection appeared to be less efficient than infection via the i.p. or s.c. route in a highly reproducible manner (Fig. 1N). Therefore, we established a reproducible protocol of *in vivo* infection with an EV71 clinical isolate (genotype B5, strain F23) by the i.p., s.c., or oral route using the NOD/SCID mouse system. The i.p. protocol was used in most of the NOD/SCID studies described below.

Next, we examined the growth kinetics of the inoculated EV71 in different tissues at different time points postinoculation (Fig. 2A to H). Viral RNA extracted from various tissues was measured by RT-qPCR analysis using GAPDH as an internal control, and infectious virus titers were measured by standard plaque formation assays using human rhabdomyosarcoma (RD) cells (see Materials and Methods). Interestingly, we observed two general phenomena in most tissues. (i) Viral titers tended to decline on day 2 in all eight tissues examined, and viral RNA levels tended to decline on day 3 in most tissues, except for the kidney and heart. In the kidney (Fig. 2C), the rapid drop in viral RNA levels occurred earlier, on day 2 instead of day 3. In the heart tissue (Fig. 2D), we observed no decline in the level of viral RNA throughout the time course. In general, the decline in infectivity (as measured by PFU) appeared to precede the decline in the viral RNA level. We also noted that in muscle and brain (Fig. 2F and G), there were small peaks of viral RNA at 2 dpi. Unlike intestine, spleen, and kidney tissues, muscle and brain are anatomically distal to the i.p. injection site. Therefore, the viral RNA titers in the brain and muscle at 1 dpi were very low. In the first round of "tug of war" between the host defense mechanism and the replicating virus in the brain and muscle, at 2 to 3 dpi, the host defense of immunodeficient NOD/SCID mice enjoyed a transient victory over the invading virus. However, in the second round of "tug of war," after 3 dpi, the replicating virus began to take off. Overall, such a "fall-and-rise" pattern of viral titers and viral RNA levels in most tissues at earlier time points postinoculation strongly suggests an attempt by an unknown host system to clear the input virus (tissue culture derived) at the initial phase of viral infection. The subsequent trend of steady increases in viral titers and RNA levels postinfection provides strong support for *in vivo* EV71 replication in NOD/SCID mice. (ii) At later time points before death (8 to 11 dpi), infectious viral titers dropped to very low or undetectable levels in most tissues, except for the spleen (Fig. 2B) and muscle (Fig. 2F).

A

Mouse strain	Route	Limb paralysis	Death
ifnar KO	i.p	-	-
	s.c	-	-
	oral	-	-
* *ifngr* KO	i.p.	+	+
FVB	i.p	-	-
	s.c	-	-
	oral	-	-
** *stat1 KO*	i.p	+	-
	s.c	-	-
NOD/SCID	i.p	+	+
	s.c	+	+
	oral	+	+

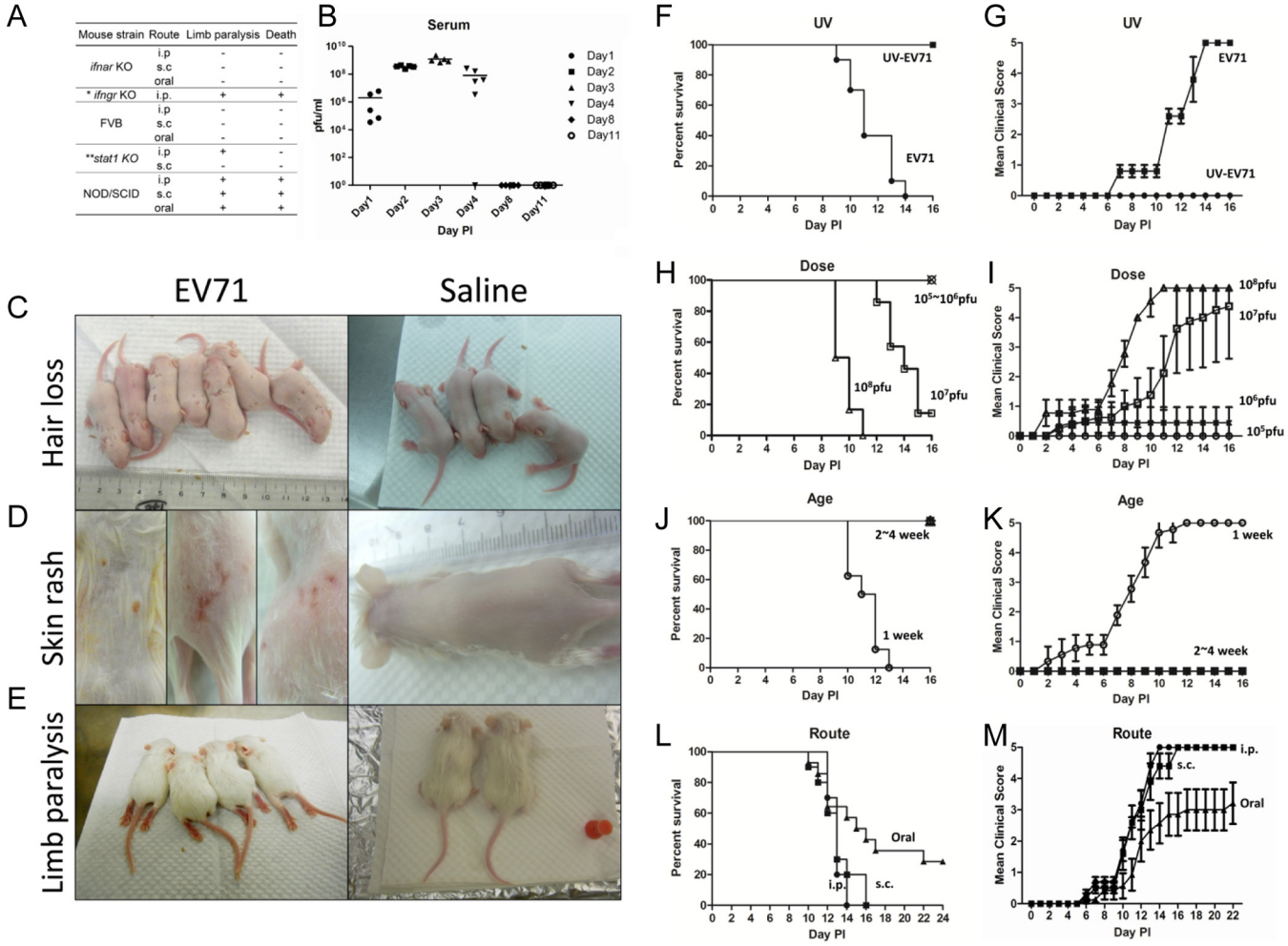

N

Dose (pfu)	i.p. infection			Oral infection		
	Skin lesion or hair loss (%)	Limb weakness or paralysis (%)	Death (%)	Skin lesion or hair loss (%)	Limb weakness or paralysis (%)	Death (%)
10^5	0/6 (0)	0/6 (0)	0/6 (0)	Not Done	Not Done	Not Done
10^6	0/6 (0)	0/6 (0)	0/6 (0)	Not Done	Not Done	Not Done
10^7	0/30 (0)	30/30 (100)	29/30 (97)	0/10 (0)	0/10 (0)	0/10 (0)
10^8	16/45 (36)	45/45 (100)	45/45 (100)	2/14 (14)	10/14 (71)	10/14 (71)

FIG 1 Studies on various parameters that affect disease manifestations in immunodeficient mice infected with a clinical isolate of EV71 (strain F23, genotype B5). (A) Comparisons among various immune-deficient mouse models infected with EV71 via different routes (*, limb paralysis rate of ~78%; **, limb paralysis rate of ~31.3%). (B) One-week-old NOD/SCID mice were infected with 10^8 PFU of EV71 strain F23. Serum samples were collected from a group of five mice on days 1, 2, 3, 4, 8, and 11, respectively. Virus titers in serum were measured by plaque assays. (C through E) One-week-old NOD/SCID mice were infected with EV71 strain F23 (left) or normal saline (right). Disease manifestations, including hair loss (C), skin rash (D), limb paralysis (E), and death, were monitored daily. (F through M) Comparisons were made for different parameters of infection, including UV treatment (or no treatment) of EV71 (F and G), viral dose ($\leq 10^6$ versus 10^7 to 10^8 PFU/mouse) (H and I), host age (1 week versus 2 to 4 weeks) (J and K), and inoculation route (i.p., s.c., or oral) (L and M). Clinical scores were defined as follows: 0, healthy; 1, hair loss, wasting, or ruffled hair; 2, limb weakness; 3, paralysis in only 1 limb; 4, paralysis in 2 to 4 limbs; 5, death. Error bars indicate standard deviations for 6 mice in each group. (N) Summary of disease manifestations in NOD/SCID mice infected with EV71 at different viral doses and through different routes.

In sharp contrast, viral RNA levels at 8 to 11 dpi declined only slightly in the spleen and brain and kept increasing in other tissues. This discrepancy between infectious viral titers and viral RNA levels seems to be paradoxical, and we interpret it as due to the significantly delayed clearance of noninfectious viral RNA relative to the more-rapid clearance of infectious virus, which was observed in the earlier phase at 2 to 3 dpi. These noninfectious viral RNAs could originate from infectious virus that was inacti-

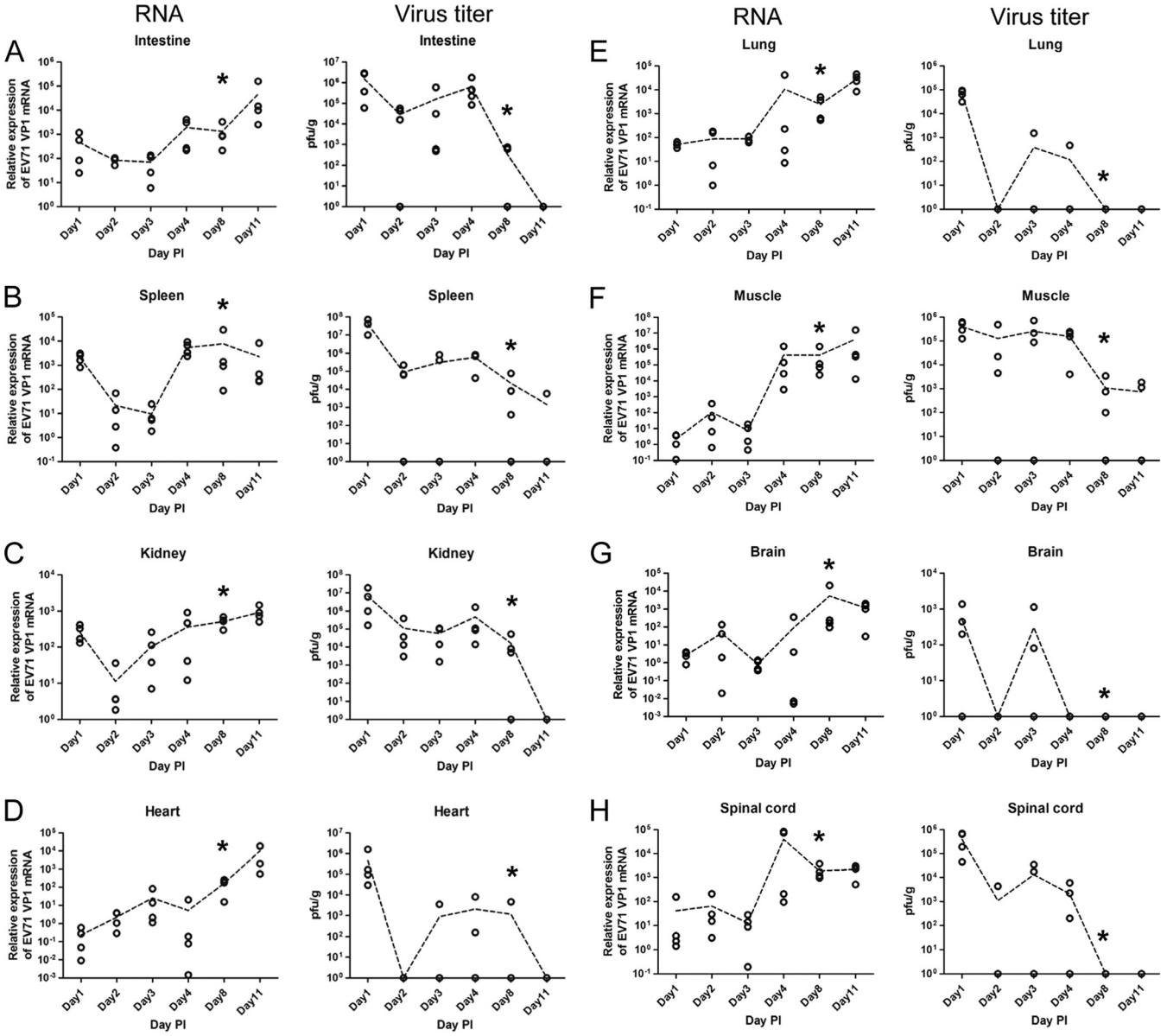

FIG 2 "Fall-and-rise" pattern of viral RNA levels and infectious titers of EV71 at earlier time points postinoculation in various tissues of EV71-infected NOD/SCID mice. One-week-old NOD/SCID mice were infected i.p. with 10^8 PFU of EV71 strain F23. On different days postinfection, mice were sacrificed. Viral RNA levels (left) and virus titers (right) in the intestine (A), spleen (B), kidney (C), heart (D), lung (E), muscle (F), brain (G), and spinal cord (H) were determined by quantitative RT-PCR and plaque assays. Fold changes of viral RNA copy numbers were detected by VP1 primers and were normalized by GAPDH primers. The virus titer in each tissue was normalized by the weight (in grams) of dissected tissues. Dashed lines connect the average data points at the different time points (see the text for further discussion). Asterisks indicate the time points of disease onset.

vated by cytokines released during inflammation (see Discussion). We speculate here that the amplification of viral titers before the point of disease onset was reached could explain why the kinetics of clearance of viral RNA lagged far behind that for infectious virus. In other words, clearance of noninfectious viral RNA could have been observed if the infected NOD/SCID mice had survived longer.

We examined sectioned EV71-infected and mock-infected tissues by H&E staining. The most-apparent pathologies were noted in the spleen, muscle, spinal cord, and skin (Fig. 3A). In the spinal cord, shrunken neurons with dark nuclei (indicated by arrows) were consistent with degenerated neurons. In contrast to the control, infected muscle was atrophic and irregular in size. We noted vacuoles (indicated by arrowheads) in the dermises of infected mice with skin lesions, suggesting inflammation-related edema. The spleens of infected mice revealed extensive dense collagen bands on H&E-stained sections, indicative of fibrosis, which was confirmed by Masson's trichrome staining (Fig. 3B, blue deposits). Spleen atrophy was revealed by the reduced sizes (Fig. 3C, left) and weights (Fig. 3C, right) of the dissected spleens of EV71-infected NOD/SCID mice. EV71-encoded VP1 protein can be detected by a brown color in the spleen, muscle, and skin by use of immunohistochemical (IHC) staining with an anti-VP1 polyclonal antibody (Fig. 3D). We also detected a cell surface marker

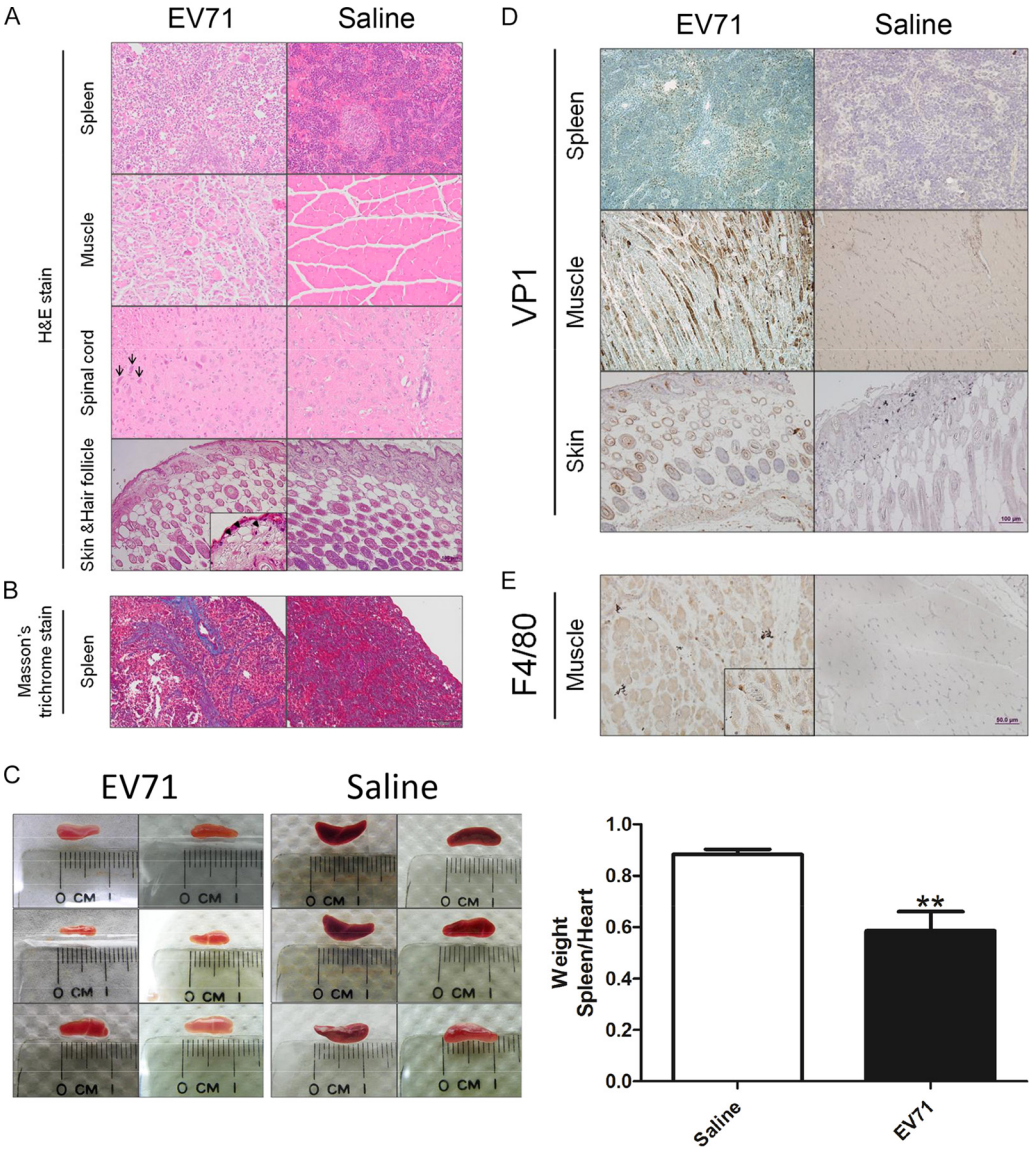

FIG 3 Pathological changes in EV71-infected NOD/SCID mice. One-week-old NOD/SCID mice were infected i.p. with 10^8 PFU of EV71 or normal saline. Moribund mice were sacrificed on day 12 postinfection. Paraffin-embedded sections were examined at ×200 with H&E stain (A), Masson's trichrome stain (B), anti-EV71 VP1 (D), and anti-F4/80 (E). (A) Multiple blue-stained cells in muscle could represent infiltrated macrophages (see panel E). Arrows (spinal cord) indicate degenerated neurons. Arrowheads (skin and hair follicle, inset) highlight vacuous edema at a magnification of ×400. (B) Blue color indicates collagen deposits and spleen fibrosis. (C) (Left) Spleen atrophy was observed on day 11 postinfection. (Right) The weights of dissected spleens from infected mice were determined and normalized to the weights of their hearts. Values are means ± standard deviations for 6 mice in each group. Asterisks indicate a significant difference (**, $P < 0.01$) from the saline control by Student's *t* test. (D) IHC staining detected VP1 protein in the spleen, muscle, and skin and hair follicles. (E) Muscle-infiltrated macrophages can be visualized by IHC using an anti-F4/80 antibody.

of infiltrating macrophages by using an anti-F4/80 monoclonal antibody (Fig. 3E). Using antibodies specific for keratin 6, keratin 14, and pan-collagen, we performed IHC staining of skin sections and detected no apparent difference in the expression of keratin and collagen between infected mice and mock-infected controls (see Fig. S2 in the supplemental material).

We compared the hematological characteristics of infected mice and mock-infected controls by complete blood counts (see Materials and Methods) and detected no significant differences in platelets and monocytes (data not shown), minor differences in mean cell volume (MCV), mean cell hemoglobin (MCH), and red blood cell volume distribution width (RDW), and more-significant differences in the numbers of neutrophils, eosinophils, and lymphocytes (Fig. 4). This reduction in lymphocyte numbers is consistent with the interpretation that EV71 in the NOD/SCID system could bias the differentiation of bone marrow cells toward the myeloid over the lymphoid lineage. The significantly increased neutrophil numbers and reduced eosinophil numbers also suggest a strong influence of EV71 on the myeloid differentiation pathways toward neutrophils over eosinophils.

In addition to the NOD/SCID model, we succeeded in establishing *stat-1* KO mice as a model susceptible to *in vivo* infection with a clinical isolate of EV71 (genotype B5, strain F23). Although we did not succeed in productive infection using the s.c. route, we

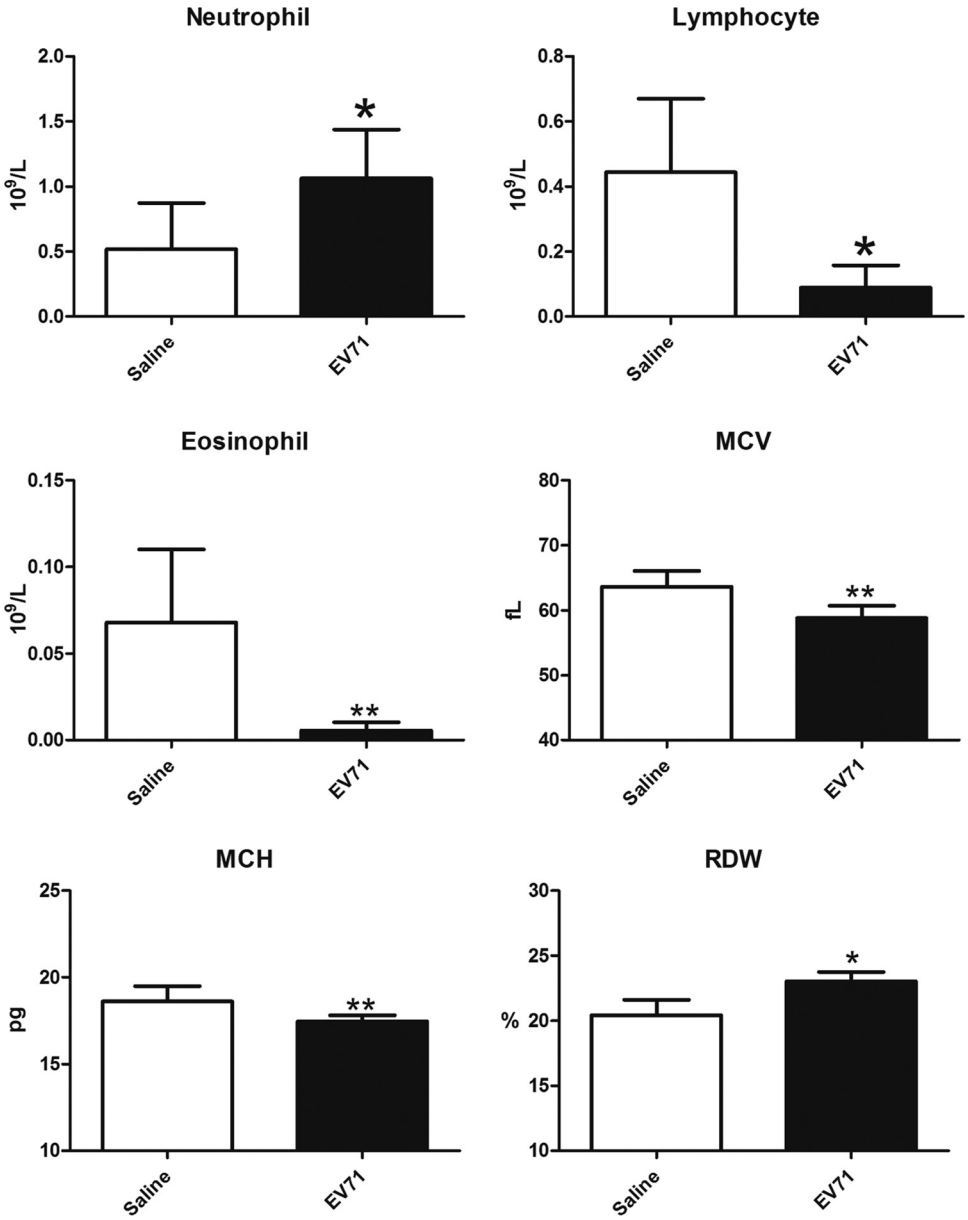

FIG 4 Hematological changes in NOD/SCID mice infected i.p. with EV71 (10^8 PFU) or injected with normal saline. Blood was collected on day 11 postinfection. Complete blood counts were recorded by an Abbott Cell-Dyn 3700 system. MCV, mean cell volume; MCH, mean cell hemoglobin; RDW, red blood cell volume distribution width. Values are means ± standard deviations for 6 mice in each group. Asterisks indicate significant differences (*, $P < 0.05$; **, $P < 0.01$) from the saline control by Student's *t* test.

observed significant clinical scores upon i.p. injection of 10^8 PFU EV71 into 1-week-old *stat-1* KO mice (Fig. 5A). Again, host age is a critical factor, since we have observed no productive infection or disease manifestation in 2-week-old mice. Approximately 30% of the infected mice developed limb paralysis around 7 dpi (Fig. 5B), and no death was observed before sacrifice up to 3 weeks postinoculation (data not shown). We observed evident pathology on H&E-stained sections from EV71-infected mice, including loss of intestinal villi, disorganized muscle structure, and spleen fibrosis (Fig. 5C). Although there was no significant pathology in the brain stem and spinal cord by H&E staining (Fig. 5C), strong expression of VP1 protein was observed by IHC staining in the pons of the brain stem, cerebellar Purkinje cells, superior colliculus, and gray matter of the spinal cord (Fig. 5D and E). In contrast to our findings for the NOD/SCID model (Fig. 3D), we detected no VP1 protein or inflammation in muscles in the *stat-1* KO model, although the muscle exhibited a certain degree of dystrophy by H&E staining (Fig. 5C and E), which could be a consequence, rather than a cause, of limb paralysis. Injury of neuronal cells is often associated with the amplification of adjacent microglial cells (24). Indeed, strong expression of IBA1, a microglial-cell marker, was detected in the brain and spinal cord by IHC staining using an anti-IBA1 antibody (Fig. 5F).

Elevated cytokine levels are known to be associated with inflammation. Previously, increased levels of various combinations of interleukin 6 (IL-6), IL-10, IFN-γ-induced protein 10 (IP-10),

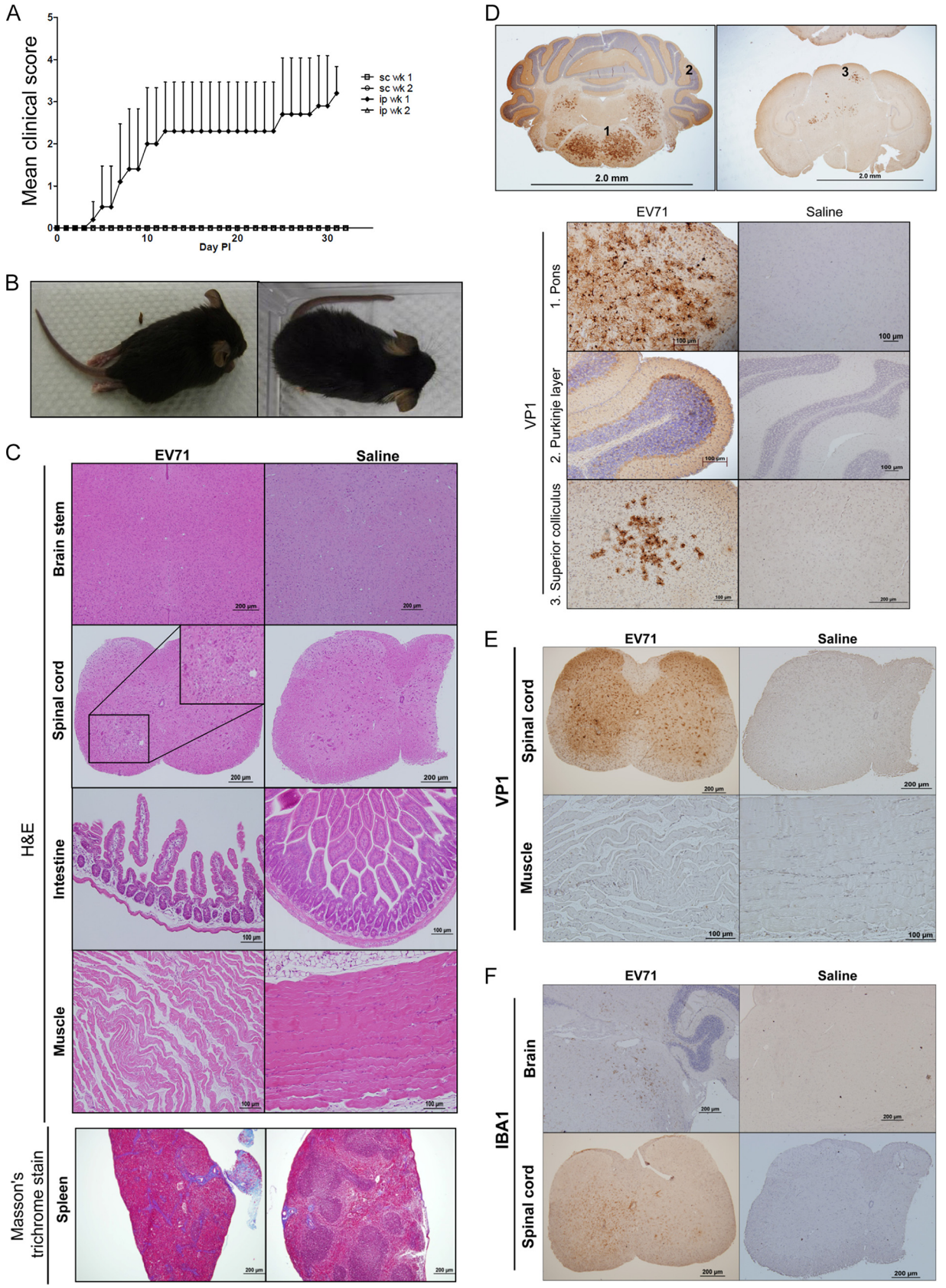

FIG 5 Symptoms of *stat-1* KO mice infected with an EV71 clinical isolate, strain F23. (A) Clinical scores of *stat-1* KO mice infected with EV71 by intraperitoneal or subcutaneous injection. (B) Limb paralysis occurred in *stat-1* KO mice infected with EV71. (Left) *stat-1* KO mouse infected with 10^8 PFU of EV71; (right)

TABLE 1 Tissue cytokine profiles in EV71-infected mouse models and human patients

Model or patient group[a]	Tissue	Cytokine profile
NOD/SCID mice	Spleen	IL-23, IL-10, TNF-α, IFN-α, MCP-1
	Muscle	IFN-γ, IL-10, IP-10, IFN-α, MCP-1, IL-1β, IL-12, TNF-α, MIP2, VEGFA
	Brain	IFN-γ, IL-10, IP-10, IL-6, MCP-1, IL-1β, IL-12, IFN-α, MIP2, VEGFA
	Spinal cord	IFN-γ, IL-10, IP-10, IL-6, MCP-1, IL-23, IL-17F, IFN-α, MIP2
stat-1 KO mice	Muscle	IFN-γ, IL-10, IFN-α
	Spinal cord	IL-17F, IFN-α, IP-10, IL-6
AG-129 mice	Serum	IFN-γ, IL-10, TNF-α, IL-6, MIP2, IL-1β
h-SCARB2-Tg mice	Brain and spinal cord	CCL-3, TNF-α, IP-10, IL-6
Patients with pulmonary edema	Serum and cerebrospinal fluid	IFN-γ, IL-10, IP-10, IL-6, MCP-1, IL-1β, TNF-α, Mig, IL-13

[a] One-week-old NOD/SCID or *stat-1* KO mice were infected i.p. with 10^8 PFU of EV71. Mice were sacrificed on 4, 8, and 11 dpi. Various tissues from the spleen, muscle, brain, and spinal cord were dissected and homogenized, and tissue cytokines were measured with a Luminex multiplex kit. Experimental results are shown in Fig. S3 and S4 in the supplemental material. See reference 12 for AG-129 mice, reference 17 for h-SCARB2-Tg mice, and reference 26 for patients with pulmonary edema.

monocyte chemoattractant protein 1 (MCP-1), and tumor necrosis factor alpha (TNF-α) were detected in the sera or tissues of EV71-infected mice or humans (12, 17, 25, 26). We examined the cytokine profiles in spleen, muscle, brain, and spinal cord tissues in the EV71-infected NOD/SCID model and in brain and spinal cord tissues in the *stat-1* KO model (Table 1; see also Fig. S3 and S4 in the supplemental material). Interestingly, the cytokine profiles in the brains and muscles of EV71-infected NOD/SCID mice exhibited a high degree of similarity to the serum cytokine profiles of EV71-infected patients with pulmonary edema; cytokines found both in patients and in NOD/SCID mice included IFN-γ, IL-1β, IL-10, IP-10, MCP-1, TNF-α (NOD/SCID mouse muscle), and IL-6 (NOD/SCID mouse brain) (26). MCP-1 and IP-10 were reported to be associated with neuronal injury in EV71-infected patients with pulmonary edema (26). IP-10 might have a certain degree of protective effect, since *ip-10* KO mice infected with a mouse-adapted EV71 variant displayed more-severe disease (27). The biological significance of specific cytokines in the NOD/SCID and *stat-1* KO models will be discussed further in comparison with that of cytokines in human patients and other mouse models.

To compare the growth kinetics of EV71 in these two mouse models more closely, we performed experimental EV71 infection of NOD/SCID and *stat-1* KO mice side by side and compared viral RNA copy numbers, infectivity, and viral protein expression in the muscle, brain, and spinal cord at different time points postinfection (before disease onset, at onset, and after onset) (Fig. 6). The viral RNA copy number increased, reached a peak around disease onset, and declined after disease onset in both models (Fig. 6A). The spinal cord of the *stat-1* KO model contained a higher copy number of viral RNA than did muscle and brain tissues at disease onset. The infectious titers of EV71 in these three tissues were also compared between these two models at different time points postinfection (Fig. 6B). Major differences in plaque-forming activity between these two models include the following: (i) at disease onset, no infectious titers could be detected in the brain and spinal cord tissues of NOD/SCID mice, and (ii) after onset, while infectious EV71 could still be detected in the muscles of NOD/SCID mice, no infectious virus was detected in the muscles of *stat-1* KO mice. We also compared viral protein expression in these two models (Fig. 6C). At disease onset, while VP1 protein was detected in the muscles of NOD/SCID mice, it was not detectable in those of *stat-1* KO mice (Fig. 6C, top). In contrast, while VP1 protein was detected in the spinal cords of *stat-1* KO mice, it was not detectable in those of NOD/SCID mice (Fig. 6C, bottom). No VP1 protein was detected in the brain tissue of either model at disease onset (Fig. 6C, center). In summary, the results shown in Fig. 6 support the general notion that the same clinical isolate of EV71 exhibited different tissue tropisms in two different mouse models: muscle tropism in the NOD/SCID model and neurotropism in the *stat-1* KO model.

It is known that *stat-1* KO mice are defective in both IFN-α and IFN-γ signaling (28, 29). Since we did not observe any disease development upon infection of *ifnar* KO mice with EV71 (Fig. 1A), we attempted to block IFN signaling *in vivo* by administering antibodies specific for both the IFN-α receptor and IFN-γ (see Materials and Methods). One-week-old wild-type C57BL/6 mice were coinjected once with 150 μg/mouse (each) of an anti-IFN-α receptor and an anti-IFN-γ antibody 1 day before inoculation with EV71 (10^8 PFU/mouse). The antibody treatment was repeated two more times after EV71 inoculation. We observed no disease development in this double-antibody experiment (data not shown). As an alternative approach, we tested the effect of IFN by using *ifngr* KO mice (30). As shown in Fig. 7, we observed a more-rapid onset of disease and death in this model than in the NOD/SCID and *stat-1* KO models (Fig. 7A and B). The death and paralysis rates for the *ifngr* KO model are generally higher than those for the *stat-1* KO model (78% versus 31%). Taking these

saline-treated control. (C) Histopathological examination of the brain, spinal cord, intestine, muscle, and spleen by staining with H&E and Masson's trichrome stain. While the brain showed no apparent pathology, the spinal cord showed some areas of higher cell density, suggesting amplification of microglia. The intestine showed loss of villi. The muscle showed some dystrophy. The blue color of the spleen section by Masson's trichrome staining represents collagen fiber and spleen fibrosis. (D) VP1 protein was expressed in the brains of EV71-infected mice as detected by IHC staining. The upper and lower panels show brain sections at a lower (×20) and a higher (×200) magnification, respectively. Numbers in the upper panels correspond to the regions of the brain with strong expression of VP1 that are shown in the lower panels: 1, pons; 2, cerebellar Purkinje layer; 3, superior colliculus. (E) Preferential VP1 expression in the gray matter, including the anterior horn, in spinal cords of EV71-infected mice. In contrast, no VP1 was detected in limb muscles. (F) Detection of the microglial marker IBA1 in the brains and spinal cords of EV71-infected mice by IHC staining. Proliferation of microglia indicates neuronal-cell injury.

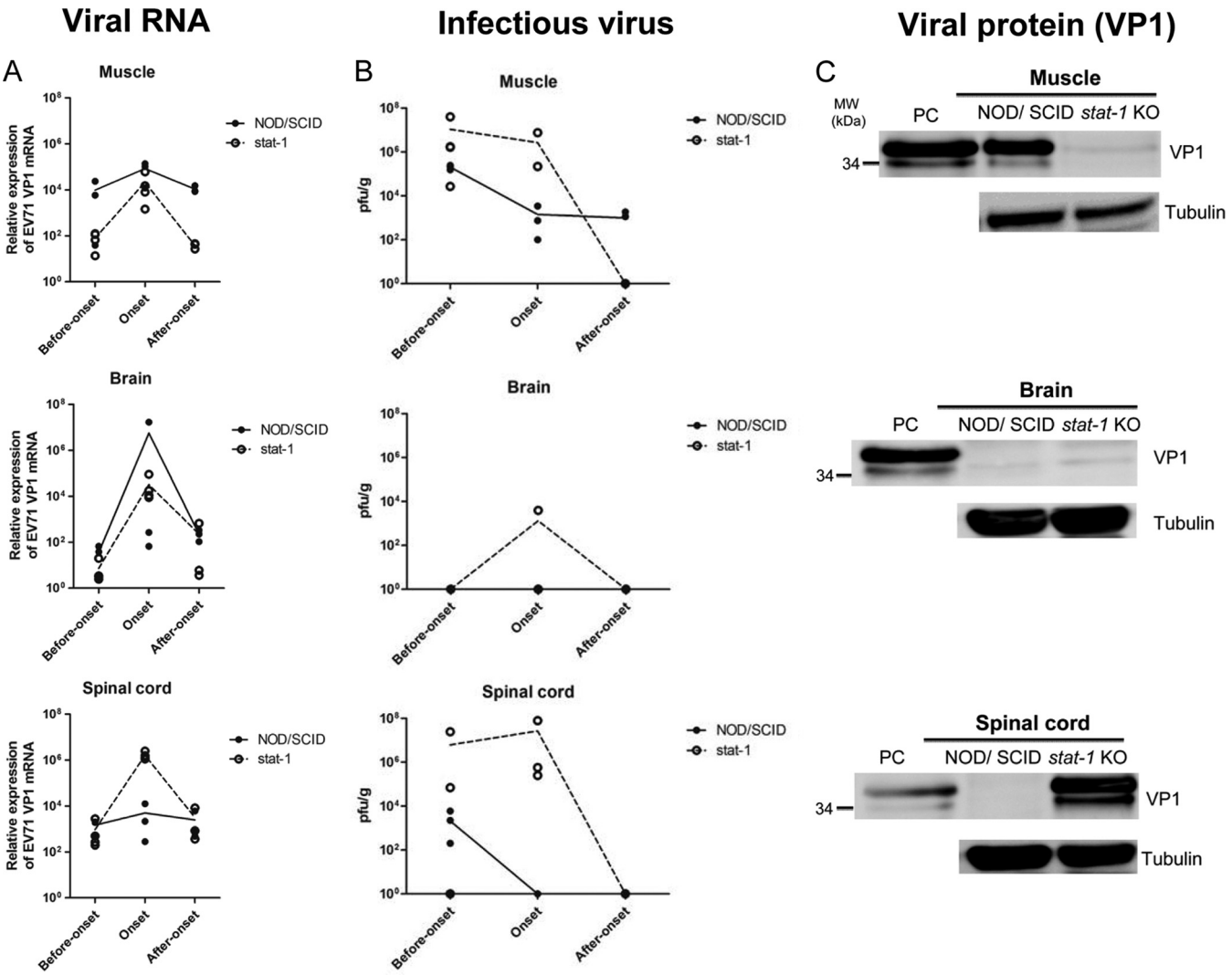

FIG 6 Side-by-side kinetic comparisons of viral RNA copy numbers, infectivity, and VP1 protein expression in muscle, brain, and spinal cord tissues between NOD/SCID and *stat-1* KO mouse models of experimental EV71 infection. One-week-old NOD/SCID and *stat-1* KO mice were infected i.p. with EV71 (10^8 PFU/mouse). Various tissues (muscle, brain, and spinal cord) were collected for analyses of total EV71 VP1 RNA expression by RT-qPCR (A), extracellular infectious virus titers by plaque-forming activity assays (see Materials and Methods) (B), and total VP1 protein expression by Western blotting (C) at three different time points (before disease onset, at onset, and after onset). Lines in the graphs connect the average data points at the different time points. (A) The general trends of the viral RNA profiles are similar for these two mouse models. Viral RNA copy numbers peaked at disease onset in both models. (B) Unlike the viral RNA expression profiles shown in panel A, the infectious titers of EV71 were different in these two models. Infectious EV71 was not detectable by the PFU assay at or after disease onset in the brains or spinal cords of NOD/SCID mice. In contrast, after onset, infectious virus could be easily detected in the muscles of NOD/SCID mice but not in those of *stat-1* KO mice. (C) At disease onset, while VP1 protein was detected in the muscles of NOD/SCID mice, it was not detectable in those of *stat-1* KO mice. In contrast, while VP1 protein was detected in the spinal cords of *stat-1* KO mice, it was not detectable in those of NOD/SCID mice. No VP1 protein was detected in the brain tissue in either model. The lower band of the VP1 doublet could represent a degradation product of the full-length protein. PC, positive control, prepared from the culture medium of EV71-infected RD cells.

findings together, IFN-γ appears to be important for protection against EV71 infection.

DISCUSSION

Here we established three models for *in vivo* EV71 infection using NOD/SCID, *stat-1* KO, and *ifngr* KO mice. Since these mice are nontransgenic and contain no putative human SCARB2 receptor for viral entry (14, 15), it is puzzling that they could support EV71 infection and replication (Fig. 1B, F, and G and 2). It is possible that mouse SCARB2, which shares 99.9% amino acid sequence similarity with human SCARB2, could serve as a surrogate receptor for viral entry, albeit at a much lower efficiency (31). In addition, the susceptibility of these mice to EV71 infection must be related to their immunodeficiency. NOD/SCID mice are deficient not only in mature T and B cells but also in NK cells (23). Unlike *stat-1* KO or AG129 mice, NOD/SCID mice are not defective in IFN signaling. The pathogenesis profiles of NOD/SCID and *stat-1* KO mice, infected with the same EV71 clinical isolate, F23, are very different and complementary to each other (see Table S1 in the supplemental material).

***In vivo* viral replication and tissue tropism in the animal models.** The rapid "fall-and-rise" pattern of viral RNA copy num-

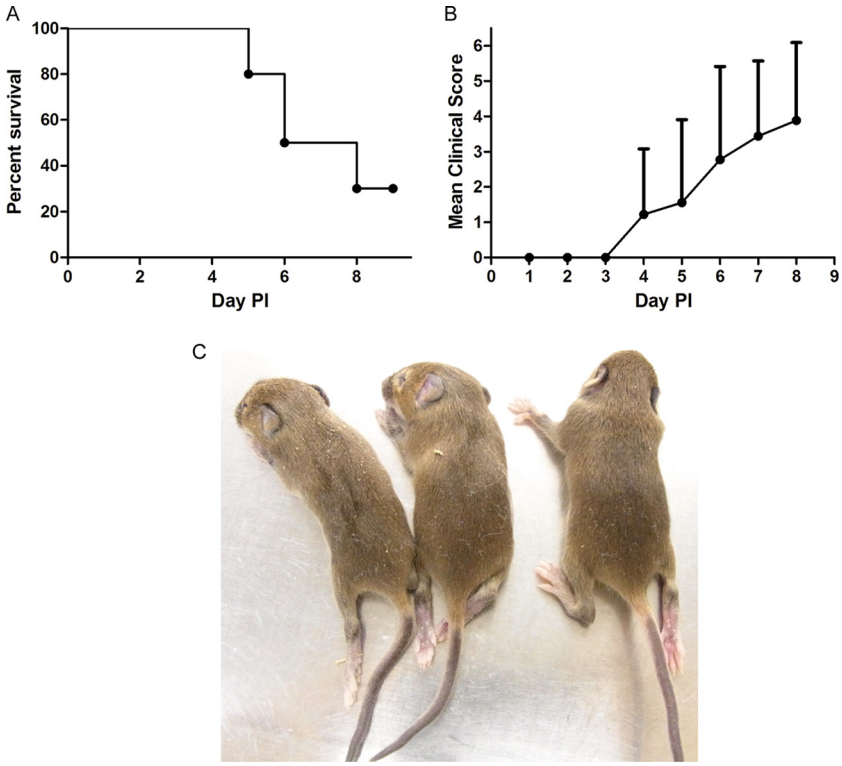

FIG 7 Time course of disease manifestations of *ifngr* KO mice after EV71 infection. One-week-old *ifngr* KO mice were injected with 10^8 PFU of EV71 F23 via the i.p. route. (A and B) The survival rate (A) and clinical score (B) were monitored daily. (C) Limb paralysis was observed at day 4 postinfection.

bers and infectious titers in most tissues in the NOD/SCID model provides strong support for active replication of EV71 *in vivo* (Fig. 2). The clearance of the infectious and noninfectious viral RNAs (e.g., defective interfering-like particles [63]) appeared to lag far behind the clearance of viral infectivity. By side-by-side comparison of the growth curves of the inoculated virus in NOD/SCID mice and *stat-1* KO mice, it became clear that viral RNA titers reached their peak at the point of disease onset in both models (Fig. 6A). In contrast to the active viral growth shown in Fig. 2 and 6, UV-inactivated virus produced no disease and no clinical score in NOD/SCID mice (Fig. 1F and G). Taken together, these results strongly suggest *in vivo* synthesis of the viral RNA genome and infectious virus titers before disease onset. The presence of infectious virus titers in the muscle at 11 dpi (Fig. 2F) and the strong presence of VP1 antigen by Western blotting at disease onset (8 dpi) (Fig. 6C) favor the notion of muscle tropism of EV71 in the NOD/SCID model. In contrast, the detection of VP1 in the brain and spinal cord by IHC (Fig. 5D and E) and in the spinal cord by Western blotting (Fig. 6C) favors the notion of neurotropism of EV71 in the *stat-1* KO model.

HFMD-like skin rash. As shown in Table 2, we compared the characteristics of several currently available mouse models for EV71 infection, including ICR mice or IP-10 knockout mice, infected with mouse-adapted EV71 variants (8, 27), SCARB2 Tg mice (16, 17), and interferon-deficient AG129 mice (12). To our knowledge, the NOD/SCID system is the only model that mimics the cutaneous lesions or skin rash of human HFMD (Table 2), which was found in about 70% of EV71-infected children with disease manifestations (1, 2, 32, 33). No skin rash was observed in previous mouse studies (8, 16, 17, 34, 35) or in the cynomolgus monkey model (11, 36). In one hSCARB2 Tg model, hair loss, but no skin rash, was observed (17). In our current NOD/SCID model, both hair loss and skin rash were detected in 36% of mice inoculated i.p. and in 14% of mice infected orally (Fig. 1N). We observed VP1 expression by IHC in hair follicles (Fig. 3D) and edema-like vacuoles in dermis (Fig. 3A) in the NOD/SCID model of i.p. EV71 infection.

Spleen fibrosis. Spleen fibrosis, identified by Masson's trichrome staining, is common in both the NOD/SCID and *stat-1* KO mouse models (Fig. 3B and 5C). However, only spleen atrophy (2, 12, 37, 38), not spleen fibrosis, has ever been reported in mouse models and humans. Whether spleen fibrosis can be detected in natural human infection deserves further investigation in the future.

Limb paralysis due to myositis or CNS involvement? EV71 infection presents two major clinical features: HFMD and neurological disorder (2). In the AG129 and hSCARB2 Tg mouse models, viral protein and injury were found in both limb muscles and the CNS (12, 17). It is therefore difficult to sort out definitively whether limb paralysis is caused primarily by muscle or CNS injury. As discussed below, we addressed this issue by using the same virus strain in two complementary models of NOD/SCID and *stat-1* KO mice.

In the *stat-1* KO model, we observed limb paralysis (30%), as well as strong expression of viral VP1 antigen (Fig. 5D and E) and inflammation (Fig. 5F, microglial IBA1 protein) only in the brain stem and spinal cord, not in the limb muscle (Fig. 5C and E). In this regard, EV71 is highly neurotropic rather than muscle tropic in the *stat-1* KO model, and limb paralysis is caused primarily by neurological disease. In contrast, in the NOD/SCID model, we

TABLE 2 Comparisons among different EV71 mouse models

Mouse strain[a]	Source of virus	Age	Dose	Infection[b] by:		Death	Limb paralysis	Skin rash	Spleen fibrosis	VP1 detection by IHC	Hematological abnormalities	Leukocyte infiltration
				Nonoral route[c]	Oral route							
ICR	Serial passage adaptive	1 day–1 wk	2×10^5–5×10^6 PFU	+	+	+	+	–	–	Brain, spinal cord	ND	ND
ip-10 KO	Serial passage adaptive	2 wk	3×10^5 PFU	+	ND	+	+	–	–	Brain	ND	ND
AG129	Clinical isolate	2 wk	5×10^5–10^7 PFU	+	+	+	+	–	–	Brain stem	ND	ND
pEF-1α-hSCARB2 Tg	Clinical isolate	1 wk	3×10^4–10^7 PFU	+	ND	+	+	–[d]	–	Brain stem, spinal cord, intestine, muscle, skin	ND	ND
pSC2-hSCARB2 Tg	Clinical isolate	3–6 wk	10^2–10^6 $TCID_{50}$	+	2/50[e]	+[f]	+[f]	–	–	Pons, medulla, cerebellar nuclei, spinal cord	ND	$CD3^+$ T cells in brain, spinal cord, intestine, lung, muscle, skin
NOD/SCID	Clinical isolate	1 wk	10^7 PFU	+	+	+	+	+	+	Spleen, muscle, skin	+[g]	Macrophages in muscle
stat-1 KO	Clinical isolate	1 wk	10^8 PFU	+	ND	–	+	–	+	Pons, Purkinje layer, superior colliculus, spinal cord	ND	ND

[a] See reference 8 for ICR mice, reference 27 for *ip-10* KO mice, reference 12 for AG129 mice, reference 17 for pEF-1α-hSCARB2-Tg mice, and reference 16 for pSC2-hSCARB2-Tg mice.
[b] ND, not done.
[c] Including the intraperitoneal, intracerebral, intravenous, and subcutaneous routes.
[d] Hair loss associated with scurf, but no skin rash.
[e] Number of mice infected/total number of mice in a total of three experiments in which 1/20, 1/20, and 1/10 mice were infected, respectively.
[f] Ataxia, paralysis, and death are defined as the same event in reference 16.
[g] See Fig. 4. The number of neutrophils and the red blood cell distribution width were increased, and the numbers of lymphocytes and eosinophils, mean cell volume, and mean cell hemoglobin were decreased, in EV71-infected mice.

obtained no direct evidence for EV71 neurotropism. Although nearly 100% of infected NOD/SCID mice developed limb paralysis, we detected no VP1 in the CNS of infected NOD/SCID mice by IHC on 4, 8, and 12 dpi (data not shown). In addition, infectious virus appeared to have been cleared from the CNS before 8 dpi (Fig. 2G and H). Given the massive destruction and strong expression of VP1 in muscle (Fig. 3A and D), but not in the CNS (data not shown), we interpreted these findings to mean that limb paralysis in the NOD/SCID model could be caused mainly by a muscle problem rather than a neurological problem. Taking our findings together, limb paralysis could be caused by either muscle or neurological injury, depending on the immunogenetic background of the host animals.

Viral spread pathways. Based on IHC staining of VP1 in the *stat-1* KO model, VP1 was strongly expressed in all levels of the spinal cord, including the anterior horn and all areas of the gray matter (Fig. 5E). In addition, we detected VP1 in the pons of the brain stem (Fig. 5D) but not in the cerebral cortex (data not shown). This result supports retrograde axonal transport from the peripheral nerves to the spinal cord ascending to the CNS, in a manner similar to that of other enterovirus systems, including mouse-adapted EV71 strains (35, 39, 40) and poliovirus (41). On the other hand, we also detected VP1 expression in a small area of the superior colliculus of the midbrain (Fig. 5D), which is not anatomically or directly connected with the spinal cord. IL-17, detected in the spinal cord (Table 1), has been reported to influence the permeability of the blood-brain barrier (42). The possibility that EV71 could somehow pass through the blood-brain barrier, perhaps at a lower efficiency, in infected mice cannot be excluded. Further investigation is needed to address this issue.

Pulmonary edema. Pulmonary edema is associated with a high mortality rate in EV71-infected patients with brain stem encephalitis (32, 43–45). In cases of bulbar poliomyelitis, fatal pulmonary edema has also been reported (46). So far, no pulmonary edema has ever been observed in any animal models of EV71 infection (12, 16, 17, 34), including our own NOD/SCID and *stat-1* KO mice (data not shown). While pulmonary edema has generally been believed to be neurogenic, the possibility that pulmonary failure could be caused in part by myositis involved in lung respiration cannot be excluded. As discussed earlier, we observed no apparent injury or viral protein in the CNS in our NOD/SCID model (data not shown); however, massive muscle damage is evident (Fig. 3A), a phenomenon similar to that reported in a recent study on pulmonary hypoventilation in 2-week-old ICR mice infected with a mouse-adapted strain of EV71 (47).

Oral infection via a natural enteric route. Inoculation with mouse-adapted strains of EV71 via the oral route can result in productive infection and disease in mice (8, 34). In the human SCARB2 Tg mouse model, neurological signs can be obtained by inoculation via the i.p. route. However, when these mice were inoculated with 10^7 50% tissue culture infective doses ($TCID_{50}$) via the intragastric (i.g.) route, only 1 out of 20 mice showed neurological signs (16). In a separate experiment using 10^8 $TCID_{50}$, no incidence of neurological signs (0/10 mice) was observed. The reason for the very low efficiency of oral infection with EV71 in the hSCARB2 Tg model (16) remains unclear. Using the IFN-α receptor KO model, we obtained no productive infection via the oral route, either (Fig. 1A). Recently, however, we succeeded reproducibly at oral infection of NOD/SCID mice (Fig. 1L to N; Table 2). Similarly, AG129 mice, defective in both IFN-α/β

and IFN-γ signaling, can be infected with EV71 via the oral route (12). While we succeeded in establishing efficient *in vivo* infection via the i.p. route using the *ifngr* KO model (Fig. 7), it remains unclear whether we can establish oral infection using this model. The potential role of IFN signaling in EV71 clearance and pathogenesis remains to be elucidated (48).

Cytokine profiles and infiltrating macrophages. We noted the striking similarity of cytokine profiles between the NOD/SCID model (muscle, brain, and spinal cord) and patients (serum and cerebrospinal fluid), including IFN-γ, IL-10, IP-10, IL-6, MCP-1, IL-1β, and TNF-α (26) (Table 1). Therefore, the NOD/SCID model, despite its immunodeficiency, could serve as an animal model resembling human EV71 infection, at least as far as cytokine profiles are concerned. In the AG129 model (12), serum IL-1β was induced by EV71 only via the oral route, not via the i.p. route. In contrast, in our studies of infection via the i.p. route, we detected IL-1β in the brain and muscle tissues of NOD/SCID mice. Furthermore, it is interesting that IL-17F was detected in the spinal cords of both EV71-infected NOD/SCID mice and EV71-infected *stat-1* KO mice (Table 1). IL-17 cytokines, including IL-17F, are known to be involved in neuroinflammation in experimental autoimmune encephalomyelitis (EAE) (49). We also detected IL-23 in the spinal cord in the NOD/SCID model (Table 1). IL-23, a member of the IL-12 family of cytokines, can promote Th17 cell development. The IL-23/IL-17 axis is well known to play an important role in various inflammatory diseases (50). Finally, the fact that we detected macrophage inflammation protein 2 (MIP2) in the CNS and muscle (Table 1), as well as F4/80 in the muscle, in NOD/SCID mice (Fig. 3E) suggests that infiltrating macrophages could contribute to inflammation and cytokine release in this model.

Gamma interferon signaling and viral infection. IFN-γ is known to exert pleiotropic effects on the immune system. In addition to its antiviral effect, IFN-γ plays an immunomodulatory role in macrophages, dendritic cells, and lymphoid cells (51–53). Mice without the IFN-γ receptor exhibited increased susceptibility to infection with *Listeria monocytogenes*, vaccinia virus (30), lymphocytic choriomeningitis virus (LCMV) (54–56), and herpes simplex virus 1 (HSV-1) (52), as well as to dengue infection-induced paralysis (57). However, IFN-γ and its receptor do not seem to be important for infection with vesicular stomatitis virus (VSV) (56, 58, 59). In the case of EV71, we demonstrated here a protective role of the IFN-γ receptor against virus-induced paralysis and death (Fig. 7).

As shown in Table 1, we detected IFN-γ in muscle, brain, and spinal cord tissues of NOD/SCID mice as well as in the muscles of *stat-1* KO mice. The absence of IFN-γ in the spinal cords of *stat-1* KO mice is consistent with the strong presence of VP1 antigen in the spinal cord by Western blotting (Fig. 6C, bottom). Similarly, the presence of IFN-γ in the brains and spinal cords of NOD/SCID mice (Table 1) could explain the absence of detectable viral antigen and pathology in their brains and spinal cords (Fig. 6C). Although IFN-γ can be detected in the muscles of NOD/SCID mice, viral RNA, viral protein, and infectious titers can be detected in the muscles of NOD/SCID mice at disease onset (Fig. 6). It is possible that the level of IFN-γ is too low to clear the virus effectively.

It remains somewhat puzzling that *stat-1*KO mice, defective in both IFN-α/β and IFN-γ signaling, had a paralysis rate of ~30% and no death, while *ifngr* KO mice, defective only in IFN-γ, not in IFN-α, displayed paralysis and death rates near 78%. Because of the difference in their respective genetic backgrounds (C57BL/6 for *ifnar* KO mice versus 129/Sv/Ev for *ifngr* KO mice), it is impossible to compare these two mouse systems at present. Another issue that may be worth discussion is that we did not succeed in inducing paralysis in our anti-IFN-γ antibody experiment (data not shown). However, *ifngr* KO mice displayed paralysis upon infection with EV71. It is possible that the blockage of a cytokine ligand may not have the same phenotype as the blockage of a cytokine receptor. For example, there appeared to be no difference in LCMV infection between IFN-γ KO mice and wild-type mice (60). However, increased susceptibility to LCMV infection was reported for *ifngr* KO mice (56).

Age-dependent susceptibility. In humans, young age is a major risk factor for natural infection with EV71 (1, 2). In animal models, young age is also a crucial determinant of productive infection, pathogenesis, and death. For example, in our NOD/SCID and *stat-1* KO models, we routinely inoculated 1-week-old mice i.p. for most studies. In other models, mice younger than 2 or 3 weeks were susceptible to EV71 infection via various routes and with various viral strains (12, 16, 17). Similarly, in one poliovirus receptor (PVR) transgenic model, 2-week-old mice were 4 orders of magnitude more susceptible to paralysis than adult mice (61). What kind of viral or host factors could contribute to the age dependency remains to be investigated; these may include the internal ribosome entry site of the virus (62) and the neonatal development of the nerve, gut, and/or immune system.

Potential for translational research. One last question to be addressed here is whether these immunodeficient mice are adequate for EV71 vaccine research. Our answer is positive, since these models can still provide an *in vivo* platform for the evaluation of vaccine efficacy by passive transfer of neutralizing antibodies. Such antibodies can be induced by vaccination in immunocompetent animals or humans. Finally, these user-friendly mouse models can be infected with clinical isolates of EV71 and thus provide an opportunity for *in vivo* testing of antivirals.

ACKNOWLEDGMENTS

We thank the Pathology Core Laboratory, Institute of Biomedical Sciences (IBMS), Academia Sinica, Taiwan for performing the staining procedures.

This work is supported by the Academia Sinica and the National Science Council, Taiwan.

REFERENCES

1. **Ho M, Chen ER, Hsu KH, Twu SJ, Chen KT, Tsai SF, Wang JR, Shih SR.** 1999. An epidemic of enterovirus 71 infection in Taiwan. Taiwan Enterovirus Epidemic Working Group. N. Engl. J. Med. **341:**929–935.
2. **Ooi MH, Wong SC, Lewthwaite P, Cardosa MJ, Solomon T.** 2010. Clinical features, diagnosis, and management of enterovirus 71. Lancet Neurol. **9:**1097–1105. http://dx.doi.org/10.1016/S1474-4422(10)70209-X.
3. **Racaniello VR.** 2007. *Picornaviridae*: the viruses and their replication, p 796–839. *In* Knipe DM, Howley PM, Griffin DE, Lamb RA, Martin MA, Roizman B, Straus SE (ed), Fields virology, 5th ed. Lippincott Williams & Wilkins, Philadelphia, PA.
4. **Feng Z, Hensley L, McKnight KL, Hu F, Madden V, Ping L, Jeong SH, Walker C, Lanford RE, Lemon SM.** 2013. A pathogenic picornavirus acquires an envelope by hijacking cellular membranes. Nature **496:**367–371. http://dx.doi.org/10.1038/nature12029.
5. **Sean P, Semler BL.** 2008. Coxsackievirus B RNA replication: lessons from poliovirus. Curr. Top. Microbiol. Immunol. **323:**89–121. http://dx.doi.org/10.1007/978-3-540-75546-3_5.
6. **Lee MS, Chang LY.** 2010. Development of enterovirus 71 vaccines. Expert Rev. Vaccines **9:**149–156. http://dx.doi.org/10.1586/erv.09.152.

7. **Lee MS, Tseng FC, Wang JR, Chi CY, Chong P, Su IJ.** 2012. Challenges to licensure of enterovirus 71 vaccines. PLoS Negl. Trop. Dis. **6:**e1737. http://dx.doi.org/10.1371/journal.pntd.0001737.
8. **Wang YF, Chou CT, Lei HY, Liu CC, Wang SM, Yan JJ, Su IJ, Wang JR, Yeh TM, Chen SH, Yu CK.** 2004. A mouse-adapted enterovirus 71 strain causes neurological disease in mice after oral infection. J. Virol. **78:**7916–7924. http://dx.doi.org/10.1128/JVI.78.15.7916-7924.2004.
9. **Li ZH, Li CM, Ling P, Shen FH, Chen SH, Liu CC, Yu CK.** 2008. Ribavirin reduces mortality in enterovirus 71-infected mice by decreasing viral replication. J. Infect. Dis. **197:**854–857. http://dx.doi.org/10.1086/527326.
10. **Arita M, Ami Y, Wakita T, Shimizu H.** 2008. Cooperative effect of the attenuation determinants derived from poliovirus Sabin 1 strain is essential for attenuation of enterovirus 71 in the NOD/SCID mouse infection model. J. Virol. **82:**1787–1797. http://dx.doi.org/10.1128/JVI.01798-07.
11. **Hashimoto I, Hagiwara A, Kodama H.** 1978. Neurovirulence in cynomolgus monkeys of enterovirus 71 isolated from a patient with hand, foot and mouth disease. Arch. Virol. **56:**257–261. http://dx.doi.org/10.1007/BF01317855.
12. **Khong WX, Yan B, Yeo H, Tan EL, Lee JJ, Ng JK, Chow VT, Alonso S.** 2012. A non-mouse-adapted enterovirus 71 (EV71) strain exhibits neurotropism, causing neurological manifestations in a novel mouse model of EV71 infection. J. Virol. **86:**2121–2131. http://dx.doi.org/10.1128/JVI.06103-11.
13. **Caine EA, Partidos CD, Santangelo JD, Osorio JE.** 2013. Adaptation of enterovirus 71 to adult interferon deficient mice. PLoS One **8:**e59501. http://dx.doi.org/10.1371/journal.pone.0059501.
14. **Yamayoshi S, Yamashita Y, Li J, Hanagata N, Minowa T, Takemura T, Koike S.** 2009. Scavenger receptor B2 is a cellular receptor for enterovirus 71. Nat. Med. **15:**798–801. http://dx.doi.org/10.1038/nm.1992.
15. **Nishimura Y, Shimojima M, Tano Y, Miyamura T, Wakita T, Shimizu H.** 2009. Human P-selectin glycoprotein ligand-1 is a functional receptor for enterovirus 71. Nat. Med. **15:**794–797. http://dx.doi.org/10.1038/nm.1961.
16. **Fujii K, Nagata N, Sato Y, Ong KC, Wong KT, Yamayoshi S, Shimanuki M, Shitara H, Taya C, Koike S.** 2013. Transgenic mouse model for the study of enterovirus 71 neuropathogenesis. Proc. Natl. Acad. Sci. U. S. A. **110:**14753–14758. http://dx.doi.org/10.1073/pnas.1217563110.
17. **Lin YW, Yu SL, Shao HY, Lin HY, Liu CC, Hsiao KN, Chitra E, Tsou YL, Chang HW, Sia C, Chong P, Chow YH.** 2013. Human SCARB2 transgenic mice as an infectious animal model for enterovirus 71. PLoS One **8:**e57591. http://dx.doi.org/10.1371/journal.pone.0057591.
18. **Huang MC, Wang SM, Hsu YW, Lin HC, Chi CY, Liu CC.** 2006. Long-term cognitive and motor deficits after enterovirus 71 brainstem encephalitis in children. Pediatrics **118:**e1785–e1788. http://dx.doi.org/10.1542/peds.2006-1547.
19. **Petersen LR, Brault AC, Nasci RS.** 2013. West Nile virus: review of the literature. JAMA **310:**308–315. http://dx.doi.org/10.1001/jama.2013.8042.
20. **Zompi S, Harris E.** 2012. Animal models of dengue virus infection. Viruses **4:**62–82. http://dx.doi.org/10.3390/v4010062.
21. **Institute of Laboratory Animal Resources, Commission on Life Sciences, National Research Council.** 1996. Guide for the care and use of laboratory animals. National Academy Press, Washington, DC.
22. **Stark GR, Darnell JE, Jr.** 2012. The JAK-STAT pathway at twenty. Immunity **36:**503–514. http://dx.doi.org/10.1016/j.immuni.2012.03.013.
23. **Shultz LD, Schweitzer PA, Christianson SW, Gott B, Schweitzer IB, Tennent B, McKenna S, Mobraaten L, Rajan TV, Greiner DL, Leiter EH.** 1995. Multiple defects in innate and adaptive immunologic function in NOD/LtSz-scid mice. J. Immunol. **154:**180–191.
24. **Vega-Avelaira D, Ballesteros JJ, Lopez-Garcia JA.** 2013. Inflammation-induced hyperalgesia and spinal microglia reactivity in neonatal rats. Eur. J. Pain **17:**1180–1188. http://dx.doi.org/10.1002/j.1532-2149.2013.00308.x.
25. **Weng KF, Chen LL, Huang PN, Shih SR.** 2010. Neural pathogenesis of enterovirus 71 infection. Microbes Infect. **12:**505–510. http://dx.doi.org/10.1016/j.micinf.2010.03.006.
26. **Wang SM, Lei HY, Yu CK, Wang JR, Su IJ, Liu CC.** 2008. Acute chemokine response in the blood and cerebrospinal fluid of children with enterovirus 71-associated brainstem encephalitis. J. Infect. Dis. **198:**1002–1006. http://dx.doi.org/10.1086/591462.
27. **Shen FH, Tsai CC, Wang LC, Chang KC, Tung YY, Su IJ, Chen SH.** 2013. Enterovirus 71 infection increases expression of interferon-gamma-inducible protein 10 which protects mice by reducing viral burden in multiple tissues. J. Gen. Virol. **94:**1019–1027. http://dx.doi.org/10.1099/vir.0.046383-0.
28. **Durbin JE, Hackenmiller R, Simon MC, Levy DE.** 1996. Targeted disruption of the mouse Stat1 gene results in compromised innate immunity to viral disease. Cell **84:**443–450. http://dx.doi.org/10.1016/S0092-8674(00)81289-1.
29. **Meraz MA, White JM, Sheehan KC, Bach EA, Rodig SJ, Dighe AS, Kaplan DH, Riley JK, Greenlund AC, Campbell D, Carver-Moore K, DuBois RN, Clark R, Aguet M, Schreiber RD.** 1996. Targeted disruption of the Stat1 gene in mice reveals unexpected physiologic specificity in the JAK-STAT signaling pathway. Cell **84:**431–442. http://dx.doi.org/10.1016/S0092-8674(00)81288-X.
30. **Huang S, Hendriks W, Althage A, Hemmi S, Bluethmann H, Kamijo R, Vilcek J, Zinkernagel RM, Aguet M.** 1993. Immune response in mice that lack the interferon-gamma receptor. Science **259:**1742–1745. http://dx.doi.org/10.1126/science.8456301.
31. **Yamayoshi S, Koike S.** 2011. Identification of a human SCARB2 region that is important for enterovirus 71 binding and infection. J. Virol. **85:**4937–4946. http://dx.doi.org/10.1128/JVI.02358-10.
32. **Lum LC, Wong KT, Lam SK, Chua KB, Goh AY, Lim WL, Ong BB, Paul G, AbuBakar S, Lambert M.** 1998. Fatal enterovirus 71 encephalomyelitis. J. Pediatr. **133:**795–798. http://dx.doi.org/10.1016/S0022-3476(98)70155-6.
33. **Shindarov LM, Chumakov MP, Voroshilova MK, Bojinov S, Vasilenko SM, Iordanov I, Kirov ID, Kamenov E, Leshchinskaya EV, Mitov G, Robinson IA, Sivchev S, Staikov S.** 1979. Epidemiological, clinical, and pathomorphological characteristics of epidemic poliomyelitis-like disease caused by enterovirus 71. J. Hyg. Epidemiol. Microbiol. Immunol. **23:**284–295.
34. **Chen YC.** 2004. A murine oral enterovirus 71 infection model with central nervous system involvement. J. Gen. Virol. **85:**69–77. http://dx.doi.org/10.1099/vir.0.19423-0.
35. **Ong KC, Badmanathan M, Devi S, Leong KL, Cardosa MJ, Wong KT.** 2008. Pathologic characterization of a murine model of human enterovirus 71 encephalomyelitis. J. Neuropathol. Exp. Neurol. **67:**532–542. http://dx.doi.org/10.1097/NEN.0b013e31817713e7.
36. **Nagata N, Iwasaki T, Ami Y, Tano Y, Harashima A, Suzaki Y, Sato Y, Hasegawa H, Sata T, Miyamura T, Shimizu H.** 2004. Differential localization of neurons susceptible to enterovirus 71 and poliovirus type 1 in the central nervous system of cynomolgus monkeys after intravenous inoculation. J. Gen. Virol. **85:**2981–2989. http://dx.doi.org/10.1099/vir.0.79883-0.
37. **Meng G-Z, Li M-Q, Li Y-Q, Wang X-M, Chen Q-Y, Wei H-S.** 2011. Severe hand-foot-mouth disease: a report of 3 autopsied cases. Chin. J. Clin. Exp. Pathol. **27:**48–51, 55.
38. **Khong WX, Foo DG, Trasti SL, Tan EL, Alonso S.** 2011. Sustained high levels of interleukin-6 contribute to the pathogenesis of enterovirus 71 in a neonate mouse model. J. Virol. **85:**3067–3076. http://dx.doi.org/10.1128/JVI.01779-10.
39. **Chen CS, Yao YC, Lin SC, Lee YP, Wang YF, Wang JR, Liu CC, Lei HY, Yu CK.** 2007. Retrograde axonal transport: a major transmission route of enterovirus 71 in mice. J. Virol. **81:**8996–9003. http://dx.doi.org/10.1128/JVI.00236-07.
40. **Wong KT, Munisamy B, Ong KC, Kojima H, Noriyo N, Chua KB, Ong BB, Nagashima K.** 2008. The distribution of inflammation and virus in human enterovirus 71 encephalomyelitis suggests possible viral spread by neural pathways. J. Neuropathol. Exp. Neurol. **67:**162–169. http://dx.doi.org/10.1097/nen.0b013e318163a990.
41. **Ren R, Racaniello VR.** 1992. Poliovirus spreads from muscle to the central nervous system by neural pathways. J. Infect. Dis. **166:**747–752. http://dx.doi.org/10.1093/infdis/166.4.747.
42. **Kebir H, Kreymborg K, Ifergan I, Dodelet-Devillers A, Cayrol R, Bernard M, Giuliani F, Arbour N, Becher B, Prat A.** 2007. Human TH17 lymphocytes promote blood-brain barrier disruption and central nervous system inflammation. Nat. Med. **13:**1173–1175. http://dx.doi.org/10.1038/nm1651.
43. **Chang L-Y, Huang Y-C, Lin T-Y.** 1998. Fulminant neurogenic pulmonary oedema with hand, foot, and mouth disease. Lancet **352:**367–368. http://dx.doi.org/10.1016/S0140-6736(98)24031-1.
44. **Wang S-M, Liu C-C, Tseng H-W, Wang J-R, Huang C-C, Chen Y-J, Yang Y-J, Lin S-J, Yeh T-F.** 1999. Clinical spectrum of enterovirus 71 infection in children in southern Taiwan, with an emphasis on neurolog-

ical complications. Clin. Infect. Dis. **29:**184–190. http://dx.doi.org/10.1086/520149.
45. **Chang LY, Lin TY, Hsu KH, Huang YC, Lin KL, Hsueh C, Shih SR, Ning HC, Hwang MS, Wang HS, Lee CY.** 1999. Clinical features and risk factors of pulmonary oedema after enterovirus-71-related hand, foot, and mouth disease. Lancet **354:**1682–1686. http://dx.doi.org/10.1016/S0140-6736(99)04434-7.
46. **Baker AB.** 1957. Poliomyelitis. 16. A study of pulmonary edema. Neurology **7:**743–751.
47. **Xiu JH, Zhu H, Xu YF, Liu JN, Xia XZ, Zhang LF.** 2013. Necrotizing myositis causes restrictive hypoventilation in a mouse model for human enterovirus 71 infection. Virol. J. **10:**215. http://dx.doi.org/10.1186/1743-422X-10-215.
48. **Kjerrulf M, Grdic D, Ekman L, Schon K, Vajdy M, Lycke NY.** 1997. Interferon-gamma receptor-deficient mice exhibit impaired gut mucosal immune responses but intact oral tolerance. Immunology **92:**60–68. http://dx.doi.org/10.1046/j.1365-2567.1997.00312.x.
49. **Kang Z, Wang C, Zepp J, Wu L, Sun K, Zhao J, Chandrasekharan U, Dicorleto PE, Trapp BD, Ransohoff RM, Li X.** 2013. Act1 mediates IL-17-induced EAE pathogenesis selectively in $NG2^+$ glial cells. Nat. Neurosci. **16:**1401–1408. http://dx.doi.org/10.1038/nn.3505.
50. **Hunter CA.** 2005. New IL-12-family members: IL-23 and IL-27, cytokines with divergent functions. Nat. Rev. Immunol. **5:**521–531. http://dx.doi.org/10.1038/nri1648.
51. **Sen GC.** 2001. Viruses and interferons. Annu. Rev. Microbiol. **55:**255–281. http://dx.doi.org/10.1146/annurev.micro.55.1.255.
52. **Bigley NJ.** 2014. Complexity of interferon-gamma interactions with HSV-1. Front. Immunol. **5:**15. http://dx.doi.org/10.3389/fimmu.2014.00015.
53. **Sturge CR, Yarovinsky F.** 2014. Complex immune cell interplay in the gamma interferon response during *Toxoplasma gondii* infection. Infect. Immun. **82:**3090–3097. http://dx.doi.org/10.1128/IAI.01722-14.
54. **Leist TP, Eppler M, Zinkernagel RM.** 1989. Enhanced virus replication and inhibition of lymphocytic choriomeningitis virus disease in anti-gamma interferon-treated mice. J. Virol. **63:**2813–2819.
55. **Klavinskis LS, Geckeler R, Oldstone MB.** 1989. Cytotoxic T lymphocyte control of acute lymphocytic choriomeningitis virus infection: interferon gamma, but not tumour necrosis factor alpha, displays antiviral activity in vivo. J. Gen. Virol. **70**(Part 12)**:**3317–3325. http://dx.doi.org/10.1099/0022-1317-70-12-3317.
56. **Müller U, Steinhoff U, Reis LF, Hemmi S, Pavlovic J, Zinkernagel RM, Aguet M.** 1994. Functional role of type I and type II interferons in antiviral defense. Science **264:**1918–1921. http://dx.doi.org/10.1126/science.8009221.
57. **Shresta S, Kyle JL, Snider HM, Basavapatna M, Beatty PR, Harris E.** 2004. Interferon-dependent immunity is essential for resistance to primary dengue virus infection in mice, whereas T- and B-cell-dependent immunity are less critical. J. Virol. **78:**2701–2710. http://dx.doi.org/10.1128/JVI.78.6.2701-2710.2004.
58. **Chesler DA, Reiss CS.** 2002. The role of IFN-γ in immune responses to viral infections of the central nervous system. Cytokine Growth Factor Rev. **13:**441–454. http://dx.doi.org/10.1016/S1359-6101(02)00044-8.
59. **Komatsu T, Reiss CS.** 1997. IFN-γ is not required in the IL-12 response to vesicular stomatitis virus infection of the olfactory bulb. J. Immunol. **159:**3444–3452.
60. **Nansen A, Christensen JP, Ropke C, Marker O, Scheynius A, Thomsen AR.** 1998. Role of interferon-gamma in the pathogenesis of LCMV-induced meningitis: unimpaired leucocyte recruitment, but deficient macrophage activation in interferon-gamma knock-out mice. J. Neuroimmunol. **86:**202–212. http://dx.doi.org/10.1016/S0165-5728(98)00055-1.
61. **Crotty S, Hix L, Sigal LJ, Andino R.** 2002. Poliovirus pathogenesis in a new poliovirus receptor transgenic mouse model: age-dependent paralysis and a mucosal route of infection. J. Gen. Virol. **83:**1707–1720.
62. **Kauder S, Kan S, Racaniello VR.** 2006. Age-dependent poliovirus replication in the mouse central nervous system is determined by internal ribosome entry site-mediated translation. J. Virol. **80:**2589–2595. http://dx.doi.org/10.1128/JVI.80.6.2589-2595.2006.
63. **Huang AS, Baltimore D.** 1970. Defective viral particles and viral disease processes. Nature **226:**325–327.